CICE 2023 Rio de Janeiro – Brazil 11TH INTERNATIONAL CONFERENCE ON FRP COMPOSITES IN CIVIL ENGINEERING

Interactive Software for Analysis and Design of GFRP Reinforced Concrete Columns per ACI 440.11-22 Code

Hayder A. Rasheed, Kansas State University, USA, hayder@ksu.edu
Ahmad Ghadban, AEDA LLC, Canada, aghadban89@gmail.com

ABSTRACT
As structural engineers become more familiar with the new ACI 440.11-22 code, it is inevitable to develop software for structural design of reinforced concrete with GFRP bars. In this paper, the development of a comprehensive interactive software for designing and analyzing circular and rectangular concrete columns reinforced with GFRP bars is presented. The program can analyze column sections subjected to biaxial bending and axial compression/tension. The software is extensively tested against an independent program developed for validation. Comparisons with experimental results are carried out. Two examples are solved highlighting similarities and differences in behavior with columns reinforced by conventional steel bars.

KEYWORDS
Design software; Internal bars; Circular columns; Rectangular columns.

INTRODUCTION

The year 2022 witnessed making history for GFRP bars by releasing the first standalone American code on designing concrete structures reinforced with this type of bars. To reap the full benefit of this relatively new development in reaching wide implementation in practice, the establishment of computational tools is inevitable to take place to facilitate tedious and demanding design calculations. At this point, very limited and primitive Excel spread sheets may be found in the engineering circles to achieve this important milestone of driving this technology from research and development stage to practical implementation. This paper is a first contribution to attend to this need by building a professional software package that enables efficient analysis and design process of a relatively involved calculation procedure for standard circular and rectangular structural concrete cross sections reinforced with GFRP bars and subjected to biaxial bending moments plus axial compression/tension.

Several experimental testing programs have been successfully conducted to examine short and slender circular columns reinforced with GFRP longitudinal and transverse reinforcement (HadHood et al. 2016, Sanni et al. 2021, Abdelazim et al. 2020). Similar experimental testing studies were published to report on short and slender square and rectangular columns reinforced with GFRP bars (Guérin et al. 2018, Khorramian 2020, Isaa et al. 2011). The above studies included the testing of columns under uniaxial bending plus axial compression. However, results of GFRP reinforced columns under biaxial bending plus axial load are missing from the literature. A brief review of the literature of engineering software inventory reveals the fact that the existing column analysis programs lack the treatment of the new topic of GFRP bar reinforcement at this point. The most prominent column analysis software packages in the market are CSI Column of Computers and Structures Inc. (2023) and SP Column of Structure Point Inc. (2023). Currently, both software packages implement steel reinforcement only into their sections. Therefore, it is not possible to adapt these two packages to employ a GFRP reinforcement scheme.

The CSI column software uses concrete stress-strain curves from Mander et al. (1988) for unconfined and confined rectangular and circular sections. There is reference to using customized constitutive behavior, but it was not possible to define arbitrary constitutive equation into the standard software package. Several built-in column cross section shapes are available. Bi-axial interaction diagrams can be computed and steel rebars can be placed anywhere in the cross-section. Effective length factor can

be calculated, and slenderness analysis is available in accordance with ACI moment magnifier method for both sway and no sway conditions. Output results include section stresses, interaction diagrams, and moment-curvature curves.

The SP column software does not specify the stress-strain model used in the formulation. Custom-built stress-strain curves are also not possible to implement. Limited built-in cross section shapes are available in the program but any custom shape can be imported. Bi-axial interaction diagrams can be computed and steel rebars can be placed anywhere in the cross-section. Effective length factors can either be provided by the user or calculated from the end conditions of the column. Slenderness analysis is available in accordance with the ACI moment magnifier method and both sway and no sway options exist. The loads and moments acting directly on the column must be provided and there is no option of defining loads on a full story frame. Output results include interaction diagrams only.

In this study, A comprehensive analysis and design software is formulated, programmed and professionally deployed to account for GFRP bars in reinforced concrete circular and rectangular columns subjected to biaxial bending and axial compression/tension. The software was benchmarked against an independent program written for this purpose as well as against experimental results available in the literature. Furthermore, comparison of the interaction diagrams developed for GFRP reinforced columns are compared against those reinforced with steel bars to examine the similarities and differences in behavior.

THEORETICAL FORMULATION

The section fails either when the strain in the extreme concrete fiber (ε_{cmax}) reaches the crushing strain (ε_{cu}) or when the strain in the extreme GFRP bar (ε_{fmax}) reaches the rupture strain (ε_{fu}). Therefore, any point on the interaction diagram corresponds to a case where both or one of the extreme points ($\boldsymbol{b/2}$, $\boldsymbol{h/2}$) and ($\boldsymbol{d' - b/2}$, $\boldsymbol{d' - h/2}$) shown in Figure 1 for rectangular cross-sections reaches ε_{cu} and ε_{fu}, respectively. Where h is the section height, b is the section width, and d' is the distance from the edge of the cross-section to the centroid of the bars.

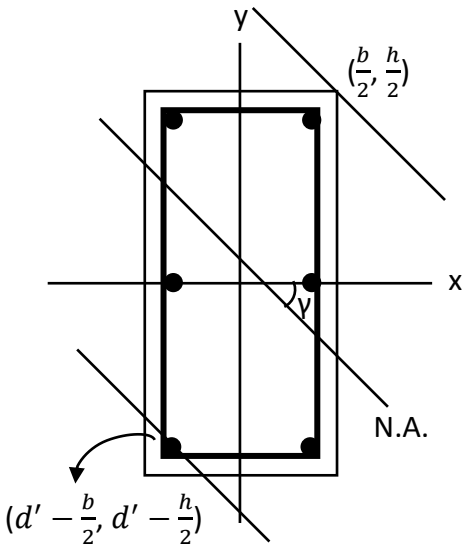

Figure 1: Concrete rectangular cross-section showing the neutral axis and points of maximum concrete and GFRP strains.

The strain in any GFRP bar or concrete element can be related to the strains at the two extreme points using strain compatibility as shown in Figure 2. The strain at any point (x_i, y_i) on the cross-section can therefore be computed according to the following equation:

$$\boldsymbol{\varepsilon_i = \frac{D_i}{D_{ext}}\left(\varepsilon_{fmax} - \varepsilon_{cmax}\right) + \varepsilon_{cmax}} \qquad \text{Eq. 1}$$

Where:

$$\boldsymbol{D_{ext} = (h - d')\cos\gamma + (b - d')\sin\gamma} \quad \text{Eq. 2}$$

$$\boldsymbol{D_i = \left(\frac{h}{2} - y_i\right)\cos\gamma + \left(\frac{b}{2} - x_i\right)\sin\gamma} \quad \text{Eq. 3}$$

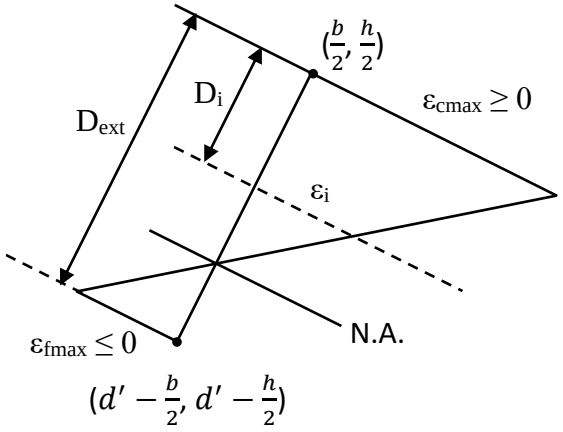

Figure 2: Strain Compatibility

For each combination of extreme points values, the corresponding axial force and biaxial bending moments can be computed by first obtaining the strain values in all GFRP bars and concrete elements. Stresses are then calculated from the stress-strain relations as follows:

$$\boldsymbol{f_{ci} = \begin{cases} f'_c\left[\frac{2\varepsilon_i}{\varepsilon'_c} - \left(\frac{\varepsilon_i}{\varepsilon'_c}\right)^2\right], & \varepsilon_i > 0 \\ 0, & \varepsilon_i \leq 0 \end{cases}, 1 \leq i \leq n} \quad \text{Eq. 4}$$

$$\boldsymbol{f_{fk} = \begin{cases} E_f\varepsilon_k, & \varepsilon_k < 0 \\ 0, & \varepsilon_k \geq 0 \end{cases}, 1 \leq k \leq n_b} \quad \text{Eq. 5}$$

Where n is the number of concrete elements and n_b is the number of GFRP bars. The axial force and biaxial bending moments corresponding to a single point on the ultimate interaction diagram are then computed as follows:

$$\boldsymbol{P_c = t_x t_y \sum_{i=1}^{n} f_{ci}\ ,\ M_{xc} = t_x t_y \sum_{i=1}^{n} f_{ci} y_i\ ,\ M_{yc} = t_x t_y \sum_{i=1}^{n} f_{ci} x_i} \quad \text{Eq. 6}$$

$$\boldsymbol{P_f = A_{bar} \sum_{k=1}^{n_b} f_{fk}\ ,\ M_{xf} = A_{bar} \sum_{k=1}^{n_b} f_{fk} y_k\ ,\ M_{yf} = A_{bar} \sum_{k=1}^{n_b} f_{fk} x_k} \quad \text{Eq. 7}$$

$$\boldsymbol{P_n = P_c + P_f\ ,\ M_{xn} = M_{xc} + M_{xf}\ ,\ M_{yn} = M_{yc} + M_{yf}} \quad \text{Eq. 8}$$

Where t_x and t_y are the dimensions of each concrete element. The resultant nominal moment and the slope angle of biaxial moment ratio are then computed as follows:

$$\boldsymbol{M_n = \sqrt{M_{xn}^2 + M_{yn}^2}} \quad \text{Eq. 9}$$

$$\boldsymbol{\alpha = \tan^{-1} M_{yn}/M_{xn}} \quad \text{Eq. 10}$$

Going through the aforementioned steps requires knowledge of the angle of the neutral axis (γ) which is unknown. Consequently, an initial value of γ must be assumed and if the computed α turns out to be

different than the desired one, a revised value of γ is then used to compute a new value of α following the same steps. This iterative process is repeated until convergence. A Newton-Raphson scheme can be used here to find γ which is the zero of the following function:

$$z(\gamma) = \tan^{-1}\frac{M_{yn}(\gamma)}{M_{xn}(\gamma)} - \alpha \qquad \text{Eq. 11}$$

It is worth noting that this iterative process is only needed for rectangular sections since the axisymmetry of circular sections eliminates the significance of α and the problem reduces to a uniaxial bending problem. The entire interaction diagram for a certain α can be constructed by computing the axial load and resultant moment corresponding to several combinations of ε_{cmax} and ε_{fmax} covering the entire range from pure compression to pure tension.

The ultimate interaction diagram can be converted to a design interaction diagram through multiplying the axial force and resultant moment by the strength reduction factor, ϕ, which depends on the value of ε_{fmax} as shown in Figure 3.

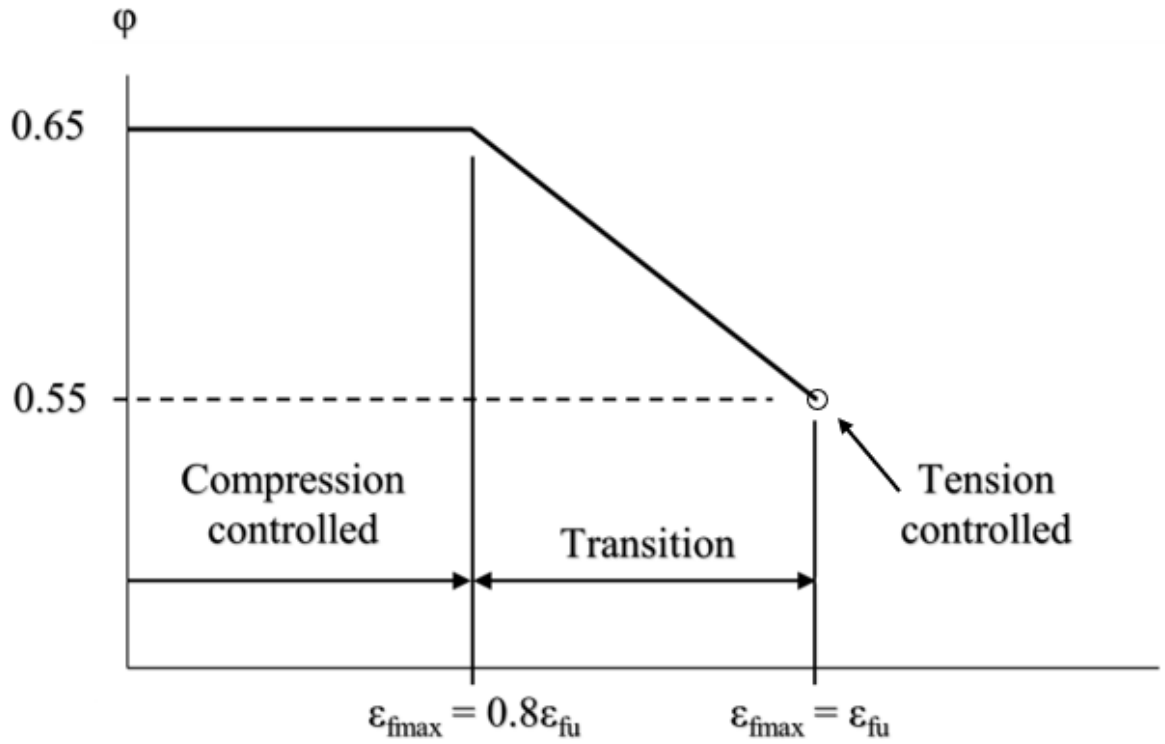

Figure 3: Variation of the strength reduction factor depending on the strain in the extreme GFRP bar (ACI 440.11-22)

All interaction points where $\varepsilon_{fmax} < -0.01$ are only plotted on the interaction diagram if the resulting axial force satisfies the following condition:

$$P_u = \varphi P_n \leq 0.1 f'_c A_g \qquad \text{Eq. 12}$$

SOFTWARE IMPLEMENTATION

The theoretical formulation was implemented into a windows form application using object-oriented programming, namely the C# programing language. The full application is capable of analyzing stub and slender columns with circular and rectangular cross sections. The inputs are collected through a user-friendly interface and processed through different methods and classes depending on the analysis function chosen by the user. For instance, if a user chooses to analyze a slender circular column, a certain method fires up and calls the appropriate classes, namely the circular section class and the

slenderness analysis class. These classes, in turn, call other classes necessary for the analysis such as the frame analysis class and the numerical analysis class.

RESULTS AND APPLICATIONS

Experimental Validations

In order to validate the design procedure described by the ACI 440.11-22 code and benchmark the accuracy of the software prediction, the test results reported by HadHood et al. 2016, Sanni et al. 2021, and Abdelazim et al. 2020 for circular columns and by Guérin et al. 2018, Khorramian 2020, and Isaa et al. 2011 for square and rectangular columns are compared to the ultimate and design interaction diagrams generated from the modelled columns using the software.

Circular Columns Group 1

Group 1 comparison is made against the columns tested in HadHood et al. (2016). The circular columns had a diameter of 305 mm and a height of 1500 mm. They were reinforced with 8#5 GFRP bars longitudinally and #3 GFRP spiral at 80 mm transversely. The three examined columns had an eccentricity of 25, 50 and 200 mm, respectively. The three failure points were mapped onto the interaction diagrams indicating accurate and slightly conservative predictions, Figure 4.

Circular Columns Group 2a

Group 2a comparison is made against the columns tested in Sanni et al. (2021). The circular columns had a diameter of 305 mm and a height of 1500 mm as well. The first series of five columns was reinforced with 8#5 GFRP bars longitudinally and #3 GFRP spiral at 80 mm transversely. The five examined columns had an eccentricity of 0, 25, 50, 100 and 200 mm, respectively. The five failure points were mapped onto the interaction diagrams indicating very accurate and slightly conservative predictions for 3 of them while the other two points were barely inside the ultimate curve, Figure 5.

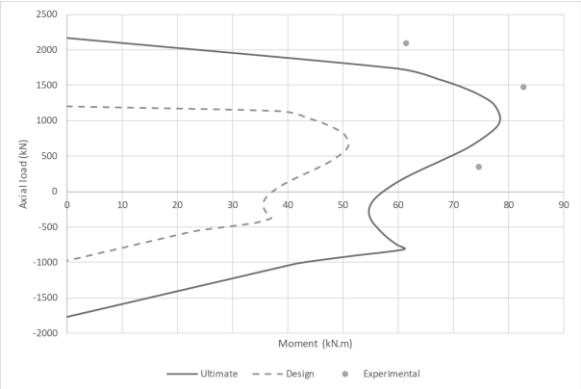

Figure 4: Circular column group 1 comparison.

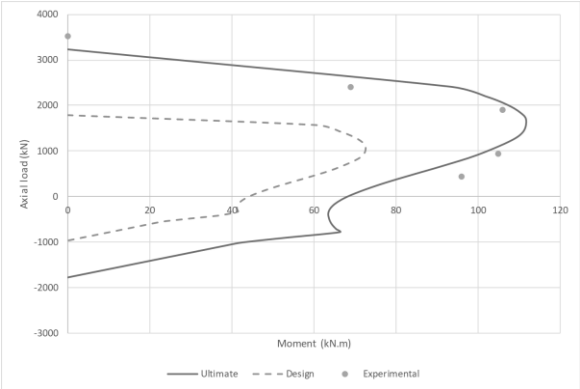

Figure 5: Circular column group 2a comparison.

Circular Columns Group 2b

Group 2b of five columns had the same column diameter and height of Group 2a. They were reinforced with 12#5 GFRP bars longitudinally and #3 GFRP spiral at 80 mm transversely. The five examined columns had the same eccentricity values as those of the first series. The five failure points were mapped onto the interaction diagrams indicating very accurate and slightly conservative predictions for 4 of them while the fifth point was inside the ultimate curve but still conservative with respect to the design curve, Figure 6.

Circular Columns Group 3a

Group 3a comparison is made against the columns tested in Abdelazim et al. (2020). This series had a diameter of 305 mm and a height of 1750 mm and 2500 mm. It was composed of twelve columns was reinforced with 8#5 GFRP bars longitudinally and #3 GFRP spiral at 80 mm for eight of them and 40 mm for the other four of them transversely. The twelve examined columns had an eccentricity range

of 0, 50, 100 and 200 mm. The twelve failure points were mapped onto the interaction diagrams indicating excellent accuracy for all points examined, Figure 7.

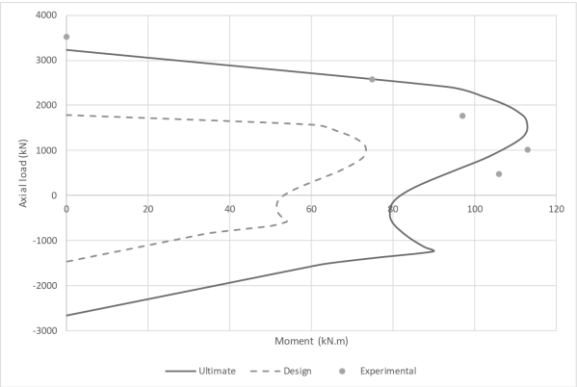

Figure 6: Circular column group 2b comparison.

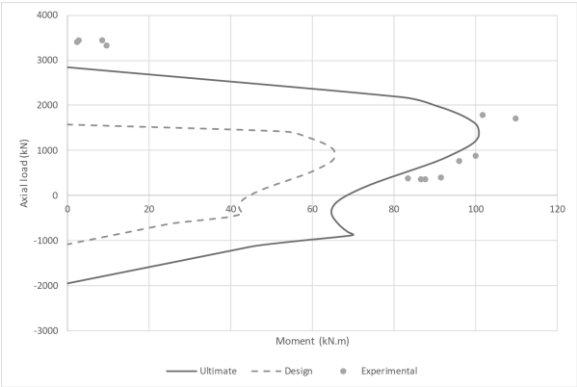

Figure 7: Circular column group 3a comparison.

Circular Columns Group 3b

Group 3b series, tested by Abdelazim et al. (2020), had a diameter of 305 mm and a height of 1750 mm and 2500 mm. This series of eight columns was reinforced with 12#5 GFRP bars longitudinally and #3 GFRP spiral at 80 mm transversely. The eight examined columns had an eccentricity range of 0, 50, 100 and 200 mm. The eight failure points were mapped onto the interaction diagrams showing excellent accuracy for all points examined, Figure 8.

Circular Columns Group 3c

Group 3c series, tested by Abdelazim et al. (2020), had a diameter of 305 mm and a height of 2500 mm. This series of two columns was reinforced with 12#6 GFRP bars longitudinally and #3 GFRP spiral at 80 mm transversely. The two examined columns had eccentricity values of 0 and 200 mm. The two failure points were mapped onto the interaction diagrams showing excellent accuracy for the points examined, Figure 9.

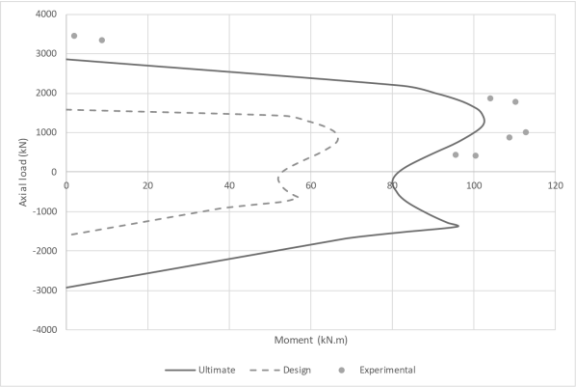

Figure 8: Circular column group 3b comparison.

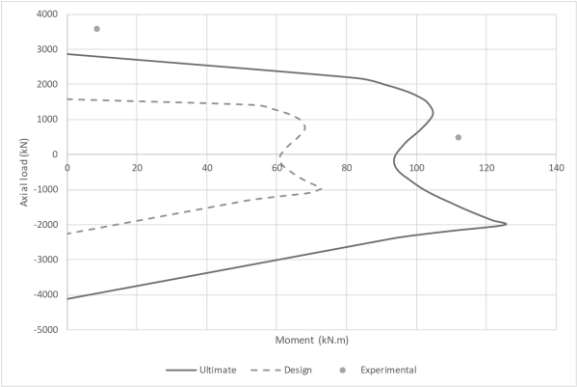

Figure 9: Circular column group 3c comparison.

Square Columns Group 4a

Group 4a comparison is made against the columns tested in Guérin et al. (2018). This series of square columns had a side dimension of 405 mm and a height of 2000 mm. They were four columns reinforced with 6#6 GFRP bars longitudinally and #3 GFRP ties at 152 mm transversely. The four examined columns had an eccentricity-to-side percentage of 10, 20, 40 and 80%, respectively. The four failure points were mapped onto the interaction diagrams indicating very accurate predictions for 3 of them while the fourth point was slightly inside the ultimate curve, Figure 10.

Square Columns Group 4b

Group 4b series of square columns, tested by Guérin et al. (2018), had a side dimension of 405 mm and a height of 2000 mm. They were four columns reinforced with 8#6 GFRP bars longitudinally and

#3 GFRP ties at 152 mm transversely. The four examined columns had an eccentricity-to-side percentage of 10, 20, 40 and 80%, respectively. The four failure points were mapped onto the interaction diagrams indicating very accurate predictions, Figure 11.

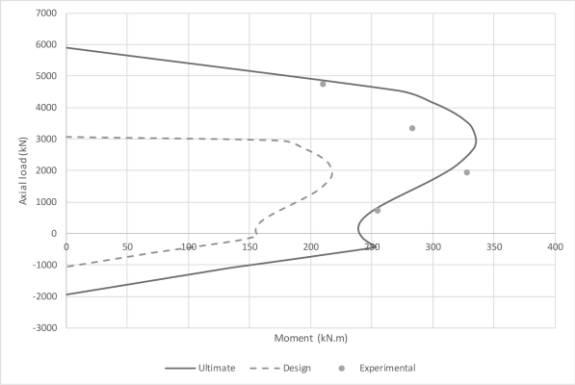

Figure 10: Square column group 4a comparison.

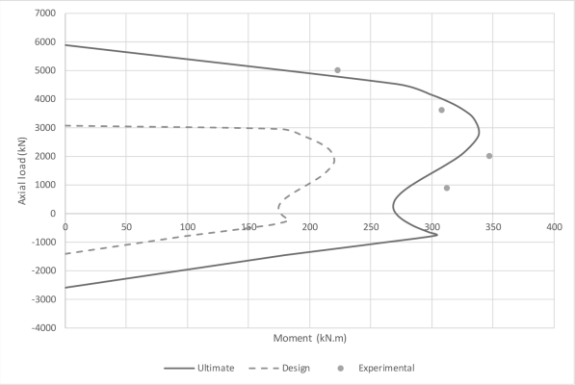

Figure 11: Square column group 4b comparison.

Square Columns Group 4c

Group 4c series of square columns, tested by Guérin et al. (2018), had a side dimension of 405 mm and a height of 2000 mm. They were four columns reinforced with 8#8 GFRP bars longitudinally and #3 GFRP ties at 203 mm transversely. The four examined columns had an eccentricity-to-side percentage of 10, 20, 40 and 80%, respectively. The four failure points were mapped onto the interaction diagrams showing superb predictions, Figure 12.

Square Columns Group 5a

Group 5a comparison is made against the columns tested in Khorramian (2020). This series of short square columns had a side dimension of 150 mm and a height of 500 mm. They were four columns reinforced with 6#5 GFRP bars longitudinally and #3 GFRP spiral at 203 mm transversely. The four examined columns had an eccentricity-to-side percentage of 0, 10, 20 and 30%, respectively. The four failure points were mapped onto the interaction diagrams indicating very conservative predictions for all four points, Figure 13.

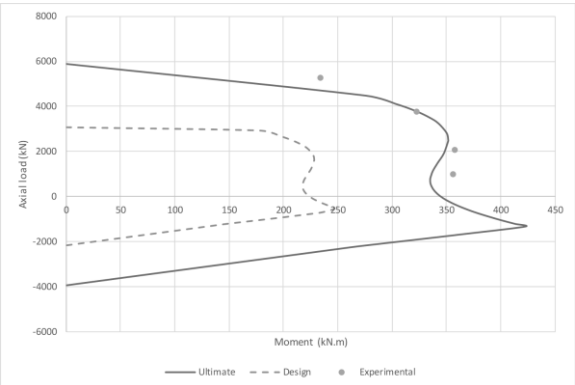

Figure 12: Square column group 4c comparison.

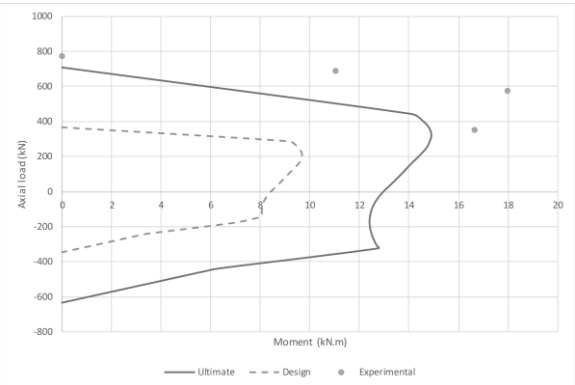

Figure 13: Square column group 5a comparison.

Rectangular Columns Group 5b

Group 5b comparison is made against other columns tested in Khorramian (2020) as well. Seven slender rectangular columns were tested with 205 x 306 mm dimensions and four different heights of 1020, 1320, 2440 and 3660 mm. They were seven columns reinforced with 10#6 GFRP bars longitudinally and #3 GFRP double ties at 150 mm transversely. The seven examined columns had two eccentricity values of 42.5 and 47.5 mm along the width, 205mm, dimension, corresponding to 21 and 23% of the width, respectively. The seven failure points were mapped onto the interaction diagrams. However, two points matched the ultimate curve perfectly while five points fell within the ultimate curve but still very conservative with respect to the design curve, Figure 14.

Square Columns Group 6

The fourth comparison is made against the columns tested in Isaa et al. (2011). Group 6 of short square columns had a side dimension of 150 mm and a height of 1200 mm. They were four columns reinforced with 4#12mm GFRP bars longitudinally and #8mm GFRP ties at 80 mm transversely. The two examined columns had an eccentricity of 50 mm. The two failure points were mapped onto the interaction diagrams indicating very conservative predictions for the two points, Figure 15.

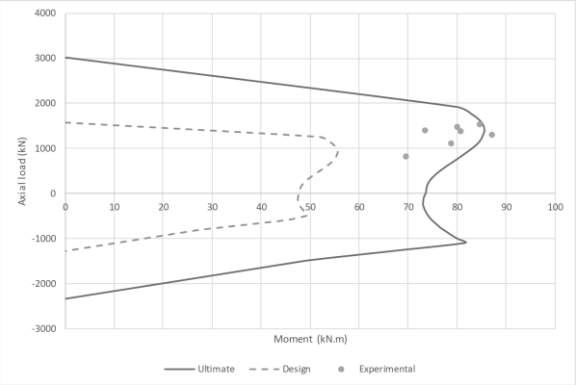

Figure 14: Rectangular column group 5b results.

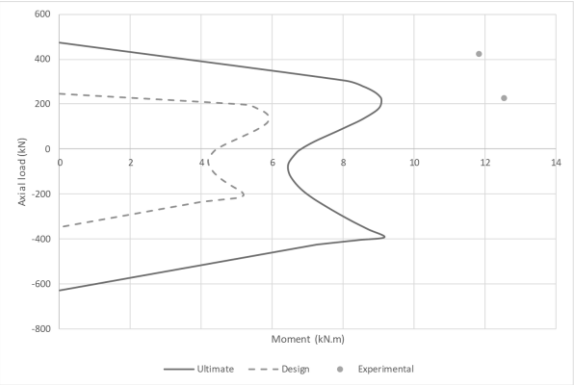

Figure 15: Square column group 6 comparison.

Comparisons Against Conventional Columns

In this section, direct comparisons of the ultimate interaction diagrams generated for identical short circular and rectangular columns reinforced with the same number of GFRP and steel longitudinal bars are made. The solutions are subjected to both ACI 440.11-22 and ACI 318-19 design limits. The similarities and differences in these envelop curves are highlighted in the following subsections.

Circular Column Sections

Two circular concrete section examples are solved in SI units to compare the interaction diagrams for a 450 mm diameter column reinforced with 8#25mm and 12#25mm GFRP and steel bars. Table 1 provides all the geometric and material parameters used in the solution. The comparison between the two interaction diagrams for each column reinforcement arrangement is shown in Figures 16-17. It is evident from the two figures that the comparison trend is generally very similar. While the columns reinforced with steel bars show higher capacity in compression due to the lack of contribution of GFRP bars in this resistance action, the capacity in tension is noticeably higher for the columns reinforced with GFRP bars due to the higher tensile strength of GFRP compared to the yielding strength of steel. On the other hand, the moment capacity at the balanced point is seen to be significantly higher for steel bars. This is attributed to the contribution of compression steel and the higher modulus of the tension steel that admits higher stresses prior to steel yielding.

Table 1: Geometric and material parameters of the circular columns.

Parameter	Example 1		Example 2	
	GFRP	Steel	GFRP	Steel
Diameter (mm)	450	450	450	450
Clear Cover (mm)	50	50	50	50
Longitudinal Bars (mm)	8#25	8#25	12#25	12#25
Spirals (mm)	#10@75	#10@75	#10@75	#10@75
Compressive Strength (MPa)	30	30	30	30
Bar Modulus (GPa)	61.7	200	61.7	200
Bar Strength (MPa)	1,172.22	414	1,172.22	414
Spiral Modulus (GPa)	63.7	200	63.7	200
Spiral Strength (MPa)	1,401.86	414	1,401.86	414

Rectangular Column Sections

One rectangular concrete section example is solved in US customary units to compare the interaction diagrams for a 12 x 20 in. column reinforced with 10#8 GFRP and steel longitudinal bars. Table 2 provides all the geometric and material parameters used in the solution. The comparison between the two interaction diagrams for the column with the biaxial moment interaction angle of α= 0°, 30°, 60° and 90° are shown in Figures 18-21. It is evident from the four figures that the comparison trend is generally similar and follow the same features observed for circular columns. Therefore, the reasoning in these cases is the same.

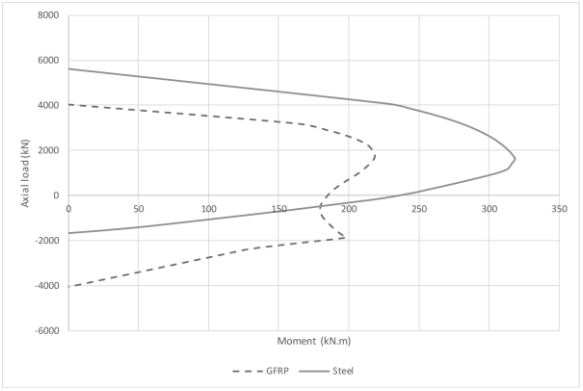

Figure 16: Example 1 column comparison.

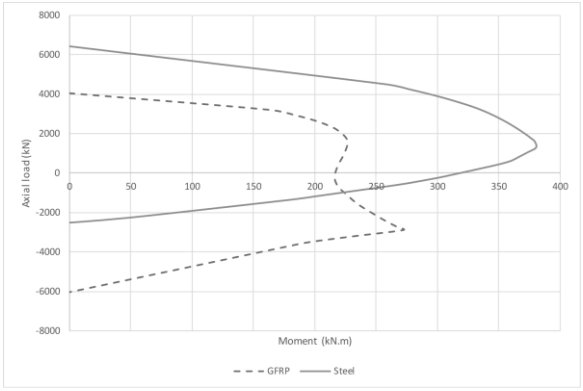

Figure 17: Example 2 column comparison.

Table 2: Geometric and material parameters of the rectangular column.

Parameter	Example 3	
	GFRP	Steel
Width (in)	12	12
Height (in)	20	20
Clear Cover (in)	2	2
Longitudinal Bars No.	10#8	10#8
Ties (in)	#3@4	#3@4
Compressive Strength (ksi)	4	4
Bar Modulus (ksi)	8,944	29,000
Bar Strength (ksi)	170	60
Spiral Modulus (ksi)	9,242	29,000
Spiral Strength (ksi)	203	60

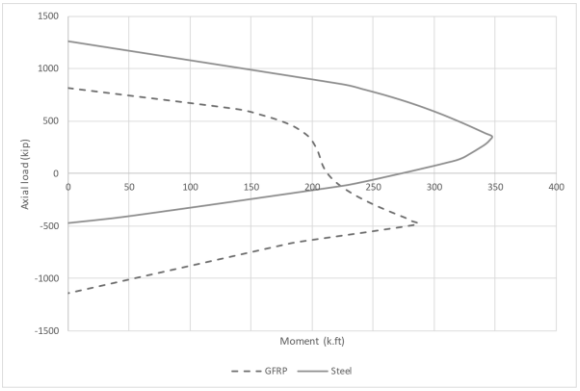

Figure 18: Example 3 comparison for α= 0°.

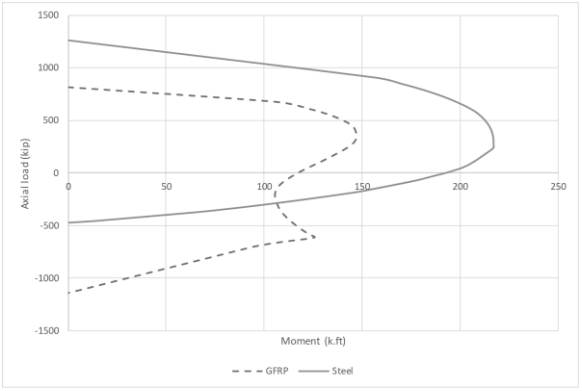

Figure 19: Example 3 comparison for α= 30°.

CONCLUSIONS

A comprehensive professional software package is developed for the analysis and design of circular and rectangular concrete columns reinforced with GFRP bars based on the provisions of ACI 440.11-22 code. The results obtained by the program are validated against an independent code. The

generated interaction diagrams are benchmarked against experimental results available in the literature showing excellent correspondence. Comparison between the behavior of circular and rectangular columns reinforced with identical GFRP and steel bars reflects the dominance of steel reinforcement in compression and the higher contribution of GFRP reinforcement in tension.

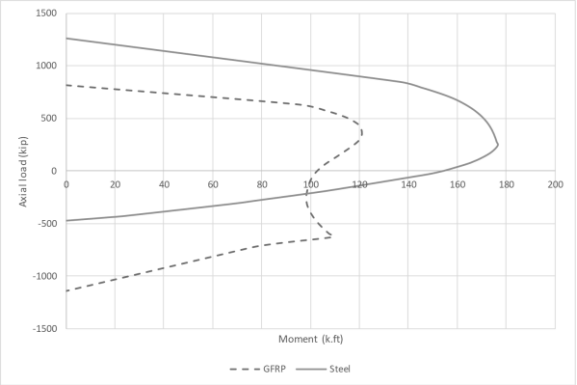

Figure 20: Example 3 comparison for α= 60°.

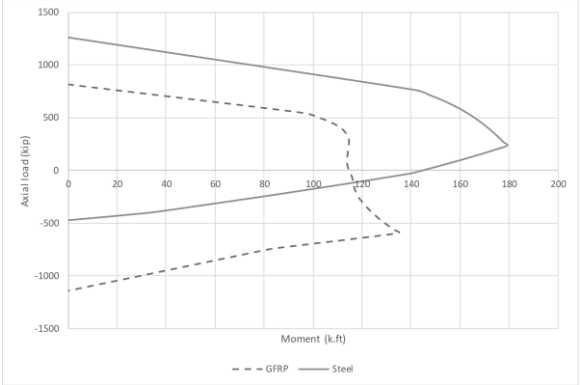

Figure 21: Example 3 comparison for α= 90°.

CITATIONS

Abdelazim, W., Mohamed, H. M., Benmokrane, B., & Afifi, M. Z. (2020). Effect of critical test parameters on behavior of glass fiber-reinforced polymer-reinforced concrete slender columns under eccentric load. *ACI Structural Journal*, *117*(4), 127-141.

ACI Committee 318, (2019). "Building Code Requirements for Structural Concrete—Code and Commentary," American Concrete Institute, Farmington Hills, MI, 2019.

ACI Committee 440, (2022). "Building Code Requirements for Structural Concrete Reinforced with Glass Fiber-Reinforced Polymer (GFRP) Bars—Code and Commentary," American Concrete Institute, Farmington Hills, MI, 2022.

Computers and Structures Inc., (2023). "CsiCol: Design of Reinforced Concrete Columns," [Online]. Available: https://www.csiamerica.com/products/csicol. [Accessed 29 May 2023].

Guérin, M., Mohamed, H. M., Benmokrane, B., Shield, C. K., & Nanni, A. (2018). Effect of Glass Fiber-Reinforced Polymer Reinforcement Ratio on Axial-Flexural Strength of Reinforced Concrete Columns. *ACI Structural Journal*, *115*(4).

HadHood, A., Mohamed, H. M., & Benmokrane, B. (2016). Behavior of circular FRP-reinforced concrete columns under eccentric loading. In *Proc. 5th Specialty Conf. on FRP structures, London, Ontario, Canada.*

Issa, M. S., Metwally, I. M., & Elzeiny, S. M. (2011). Structural performance of eccentrically loaded GFRP reinforced concrete columns. *International Journal of Civil & Structural Engineering*, *2*(1), 395-406.

Khorramian, K. (2020). Short and slender concrete columns internally or externally reinforced with longitudinal fiber-reinforced polymer composites, Ph.D. Dissertation, Dalhousie University.

Mander, J. B., Priestley, M. J., & Park, R. (1988). Theoretical stress-strain model for confined concrete. *Journal of structural engineering*, *114*(8), 1804-1826.

Sanni, B. A., Mohamed, H. M., Yahia, A., & Benmokrane, B. (2021). Behavior of Lightweight Self-Consolidating Concrete Columns Reinforced with Glass Fiber-Reinforced Polymer Bars and Spirals under Axial and Eccentric Loads. *ACI Structural Journal*, *118*(3), 241-254.

Structure Point Inc., (2023). "spcolumn: Analysis and Design of Concrete Sections," [Online]. Available: https://structurepoint.org/soft/software-profile.asp?l_family_id=63. [Accessed 29 May 2023].

ACKNOWLEDGEMENT

The authors would like to acknowledge the financial support provided by Sustainable Alliance Pty Ltd of Australia to develop the software described herein.

CONFLICT OF INTEREST

The authors declare that they have no conflicts of interest associated with the work presented in this paper.

DATA AVAILABILITY

Data on which this paper is based is available from the authors upon reasonable request.